Three-Dimensional Multitrack Electrical Conductivity Method for Interpretation of Complex Ice Core Stratigraphy

Journal:	*Journal of Glaciology*
Manuscript ID	Draft
Manuscript Type:	Article
Date Submitted by the Author:	n/a
Complete List of Authors:	Kirkpatrick, Liam; University of Washington, Earth and Space Sciences Carter, Austin; University of California San Diego Scripps Institution of Oceanography Marks Peterson, Julia; Oregon State University College of Earth Ocean and Atmospheric Sciences Shackleton, Sarah; Woods Hole Oceanographic Institution Fudge, T. J. ; University of Washington, Earth and Space Sciences
Keywords:	Ice core, Blue ice, Ground-penetrating radar, Glacier flow
Abstract:	Recent ice cores from the Allan Hills, a blue ice area in Antarctica, are nearly 3 million years old. These cores extend ice core chronologies, enabling new insight into key climate periods such as the Mid-Pleistocene Transition. The interpretation of these climate records is complex because of the disturbed stratigraphy in this ice. Here we present a new three-dimensional multitrack electrical conductivity measurement method (3D ECM) to resolve layer structure. We demonstrate this technique on a cumulative 60 m of two large-diameter (241 mm) ice cores, ALHIC2201 and ALHIC2302. We find well defined and dipping layering in both cores, averaging 28° and 68° from horizontal, respectively. Both cores show a statistically significant but gradual decrease in dip angle with depth. We discuss how this new method can be applied to enable accurate, high-resolution multi-proxy record development even in ice cores with steeply dipping layers. 3D ECM improves interpretation of blue ice area cores by providing accurate, non-destructive constraints on stratigraphy.

Three-Dimensional Multitrack Electrical Conductivity Method for Interpretation of Complex Ice Core Stratigraphy

Liam Kirkpatrick[1], Austin Carter[2], Julia Marks-Peterson[3], Sarah Shackleton[4], T.J. Fudge[1]

1. Department of Earth and Space Sciences, University of Washington
2. Scripps Institution of Oceanography, University of California San Diego
3. College of Earth, Ocean, and Atmospheric Sciences, Oregon State University
4. Woods Hole Oceanographic Institution

Correspondence: liamkp@uw.edu

ABSTRACT

Recent ice cores from the Allan Hills, a blue ice area in Antarctica, are nearly 3 million years old. These cores extend ice core chronologies, enabling new insight into key climate periods such as the Mid-Pleistocene Transition. The interpretation of these climate records is complex because of the disturbed stratigraphy in this ice. Here we present a new three-dimensional multitrack electrical conductivity measurement method (3D ECM) to resolve layer structure. We demonstrate this technique on a cumulative 60 m of two large-diameter (241 mm) ice cores, ALHIC2201 and ALHIC2302. We find well defined and dipping layering in both cores, averaging 28° and 68° from horizontal, respectively. Both cores show a statistically significant but gradual decrease in dip angle with depth. We discuss how this new method can be applied to enable accurate, high-resolution multi-proxy record development even in ice cores with steeply dipping layers. 3D ECM improves interpretation of blue ice area cores by providing accurate, non-destructive constraints on stratigraphy.

1. INTRODUCTION:

Extending ice core records beyond the 800,000-year EPICA Dome C record is the goal of multiple current and future ice coring efforts (Wolff and others, 2006; Fischer and others, 2013; Karlsson and others, 2018). Longer ice core records will provide insight into the evolution of atmospheric composition during previous climate periods such as the Mid-Pleistocene Transition (Wolff and others, 2006). Drilling in blue ice areas has emerged as a promising approach for recovering old ice at shallow depth (Spaulding and others, 2013; Higgins and others, 2015; Yan and others, 2019). Large-diameter drills can be used to obtain large sample volumes, which aids in the development of paleoclimate records in regions of highly thinned ice. The development of an argon gas dating method (Bender and others, 2008) has enabled absolute age measurements of ice, showing a complex age-depth relationship where pockets of older and younger ice are interspersed (Higgins and others, 2015; Yan and others, 2019). However, the interpretation of climate records is challenging due to the complex ice flow at the site.

Understanding the complex stratigraphy of the Allan Hills cores is critical to developing accurate, high-resolution climate records. Steeply dipping layering might result in significant age offsets across the width of the core, and folding might cause discontinuities and age reversals.

Thus, to combine multiple proxies sampled independently on an common depth scale, it is necessary to develop a high-resolution picture of layer orientations within the ice core.

There has been a variety of efforts to image layering and stratigraphy within ice cores. Visual observation (Alley and others, 1997) and optical imaging (Svensson and others, 2005; Faria and others, 2010) have been applied to assess layer stratigraphy. Line scanners (Faria and others, 2010; Jansen and others, 2016; Svensson and others, 2005; Takata and others, 2004) enable similar data to be collected efficiently over longer sections of core. These methods provide useful observations of layer structure yet are limited to two dimensions and have the best quality in clathrate ice. Recent work has demonstrated the potential to combine optical imaging with borehole instrumentation and assumptions about layer orientation to reconstruct ice core azimuth (Westhoff and others, 2021).

Electrical Conductivity Measurements (ECM) are a well-established measurement which is often a standard step in ice core processing (Hammer, 1980; Taylor and others, 1993, 1997; Wolff, 2000). The method has been applied in both Greenland and Antarctica to count annual layers in cores, for use in timescale development (WAIS Divide Project Members, 2013; Meese and others, 1997; Rasmussen and others, 2006; Taylor and others, 1993, 1997). ECM can also be used to identify acidity peaks from volcanic eruptions, which contribute to timescale development by providing tie points to other chronologies (Rasmussen and others, 2013; Severi and others, 2012). ECM has previously been applied to identify stratigraphy in two dimensions (Taylor and Alley, 2004; Fudge and others, 2016). ECM typically applies DC current, but AC current is also applied in some systems (Sugiyama and others, 2000; Taylor and others, 2004). AC-ECM is a similar measurement to di-electric profiling (DEP, e.g. Wilhelms and others, 1998; Wilhelms, 2005; Mojtabavi and others, 2020) except that the electrodes are in contact with the ice rather than surrounding it. The advantage is increased spatial resolution, while the disadvantage is that a quantitative measurement of the electrical properties is not possible.

Multitrack ECM, which measures along parallel tracks, initially enabled stacking to reduce noise (Fudge and others, 2013; Taylor & Alley, 2004; Wolff and others, 1999). Taylor and Alley (2004) followed by Fudge and others (2016) demonstrated that parallel tracks could also be used to determine the orientation of layering across the width of the measured surface. However, this two-dimensional approach was only able to ascertain the apparent dip of observed layering, rather than the true three-dimensional orientation of layers. In this paper, we present a new method to apply multitrack ECM to constrain layering in three dimensions.

2. METHODS

2.1 ALHIC2201 and ALHIC2302 ice cores

We present three-dimensional multitrack ECM (3D ECM) data from the upper sections of two new ice cores from the Allan Hills (76.73°S, 159.36°E) in Victoria Land, East Antarctica. The location of the ALHIC2201 and ALHIC2302 cores are shown in Fig. 1. Accurate dating from both cores is ongoing, though context from other cores in this area suggests the upper 50 m of these cores is hundreds of thousands of years old (Higgins and others, 2015; Yan and others, 2019). Both sites were selected to accompany existing cores (ALHIC1901 and ALHIC1902). ALHIC2201 and ALHIC2302 were both drilled with the Blue Ice Drill (BID), which provides uniquely large 241 mm (~9.5”) diameter cores (Kuhl and others, 2014).

Core quality in the upper 50 m of these cores is consistently high, with continuous ~1 m sections of ice. There is evidence of fine fracturing in the upper ~10 m of both cores, possibly from thermal expansion/contraction in the shallowest ice. These fractures impacted ECM measurement in the upper 10 m of ALHIC2201; therefore, we assumed ALHIC2302 would be similarly impacted and did not complete ECM measurements on the upper 10 m of that core. To reduce transport logistics, these cores were cut in the field. Fig. 2 shows the cut plan for the upper sections of both cores, along with the location of ECM measurements. 3D ECM measurements were completed from 0 to 22.8 m depth in ALHIC2201, and from 8.5 to 46.4 m depth in ALHIC2302.

In the field, an initial marking was made on the ice surface using a graphite stick, and the corresponding azimuth was measured relative to true north using a compass. After the first ice core section was drilled, an orientation line was marked along the core depth using this initial marking. As each section of core was subsequently recovered, core handlers aligned it with the previous section and continued the orientation line down the length of the new core section. The position of this mark is shown in Fig. 2. When the orientation line could be transferred between core sections, the azimuth of each section was the same as the one immediately above it. However, fractured core breaks resulted in difficulty transferring the orientation line between some core sections, and so a possible change in the relative position of the orientation line. The compass azimuth of the orientation line was measured at the surface of ALHIC2201 and is maintained through a depth of 17 m. The azimuth of the ALHIC2302 orientation line was not measured.

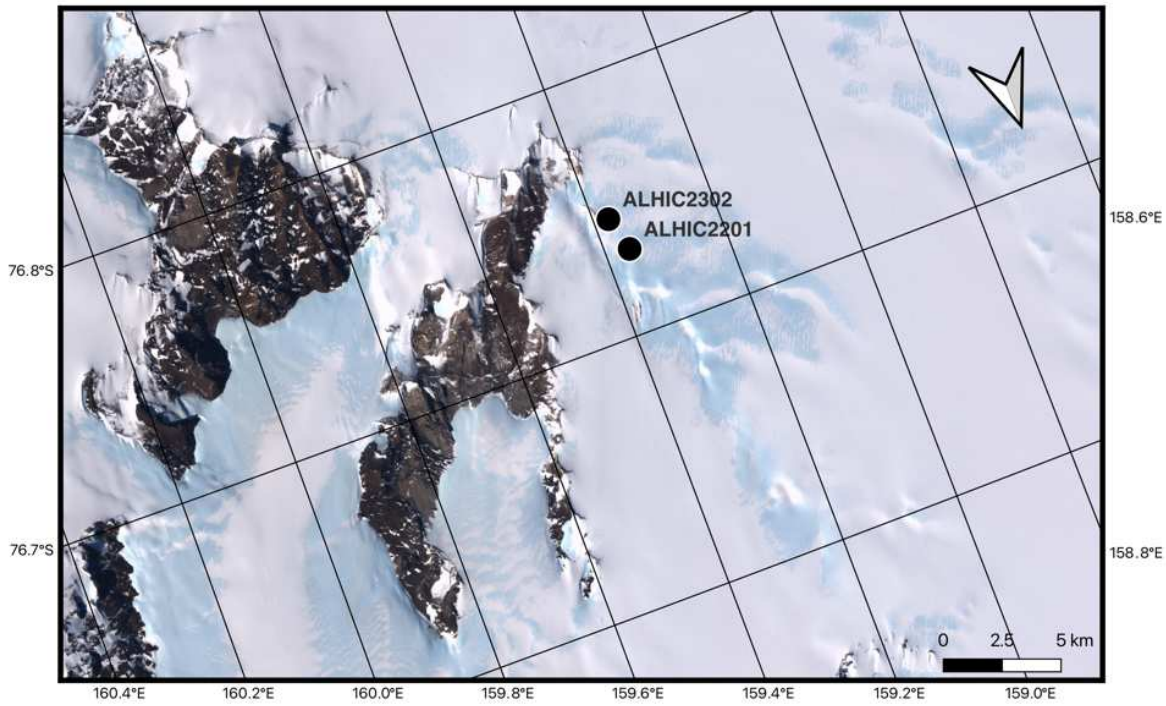

Figure 1. Location of ALHIC2302 and ALHIC2201 in the Allan Hills blue ice area. Figure uses Landsat Image Mosaic of Antarctica data (Bindschadler and others, 2008) for a true-color representation of the region. Grid north is up, and true north is indicated by the arrow.

2.2 3D ECM instrument

We have updated the ECM instrument to be compatible with large-diameter ice cores. The fundamental elements of this instrument were described by Taylor and others (1997) and Taylor and Alley (2004). The system can support direct current ECM (DC-ECM) and alternating current ECM (AC-ECM). DC-ECM uses a constant 1000 V DC potential difference between a pair of electrodes, while the AC-ECM system uses a larger pair of electrodes and a 100 kHz 2 V potential difference. This study uses the AC-ECM data because the larger electrodes result in less noise being introduced by the large bubbles in these relatively shallow ice cores.

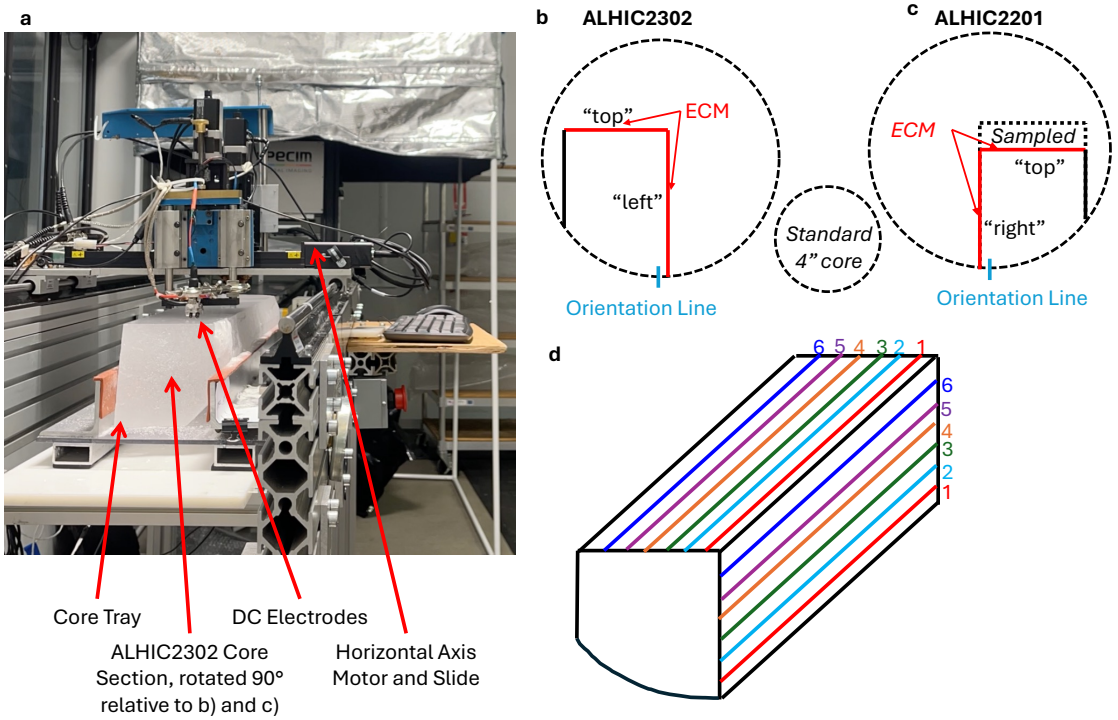

Figure 2. (a) A section of ice from ALHIC2302 being scanned for electrical conductivity. The DC electrodes are pressed against the ice surface, measuring track 2, while the AC electrodes are hidden behind them. This section of ice is rotated 90° counterclockwise around the depth-axis relative to its orientation in reference diagrams in (b) and (d), to enable measurement of the "left" face. (b) and (c) show a cross section, where depth increases out of the page, of the cut from both ALHIC2302 and ALHIC2201 large-diameter cores. A cross section of the smaller, standard ~4" core is shown for scale. The "top," "left," and "right" ECM face nomenclature is also shown. (d) A three-dimensional representation of ALHIC2302 depicting the six AC- and DC-ECM tracks.

Hardware and software improvements to the ECM system enable 3D ECM on large-diameter cores. The instrument now facilitates mm-accurate positioning in the cross-track dimension as well as the depth dimension, enabling alignment of perpendicular faces in three-dimensional space. The measurement process is to first measure one face in both AC and DC, and then rotate the ice 90° and measure a perpendicular face, as shown in Fig. 2. Completing 1 m of AC and DC 3D ECM on a quarter section of a 241 mm diameter core at 15 mm track

separation takes approximately one hour with a single operator. Between 25 to 30 meters of high-quality core can be measured in a week. The increase in time per core relative to previous ECM techniques is due to the following: 1) measuring wider cores; 2) increased setup time to get 3D positioning; and 3) repositioning each core between measurement of each face. An example of the resulting 3D ECM data is shown in Fig. 3. The large diameter BID ice cores help accommodate the perpendicular faces necessary for 3D ECM; applying 3D ECM on standard ~4" cores would require careful cut plans to provide two perpendicular faces of enough width to resolve layering.

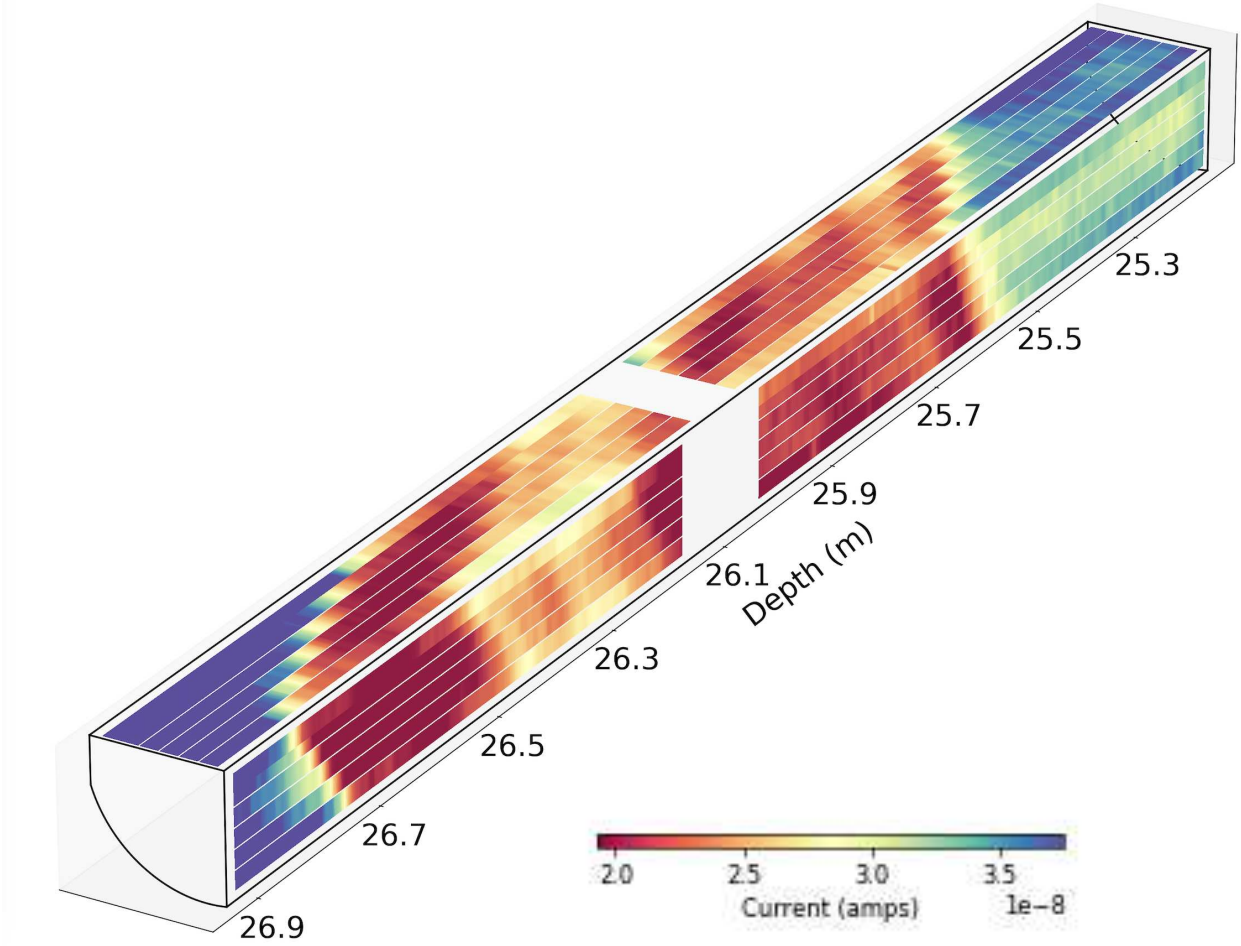

Figure 3. Two core sections of AC 3D ECM data from ALHIC2302 from 25.1 to 26.9 m in depth with strong ECM layering. Depth increases to the bottom left. The diagram shows both faces of a quarter-core cut, with the white gap representing the short gap between sections which could not be measured with 3D ECM. Note the well-defined and steeply dipping layering.

2.3 Three-dimensional orientation calculation

After two-dimensional multitrack AC-ECM data has been collected on two perpendicular faces, it is possible to calculate the dip and dip direction. We use the following terminology:

- *Apparent dip*: the inclination of observed layering as seen in a single plane, which must be less than or equal to the dip
- *Dip*: the inclination of observed layering from the horizontal plane (between 0° and 90°).

- *Dip direction*: the direction of steepest descent relative to an orientation line drawn on the core (between 0° and 360°). Note that this is distinct from the azimuth of the dip direction.
- *Azimuth*: the direction relative to true north, here applied to both the orientation line and the direction of steepest dip (azimuth of dip).

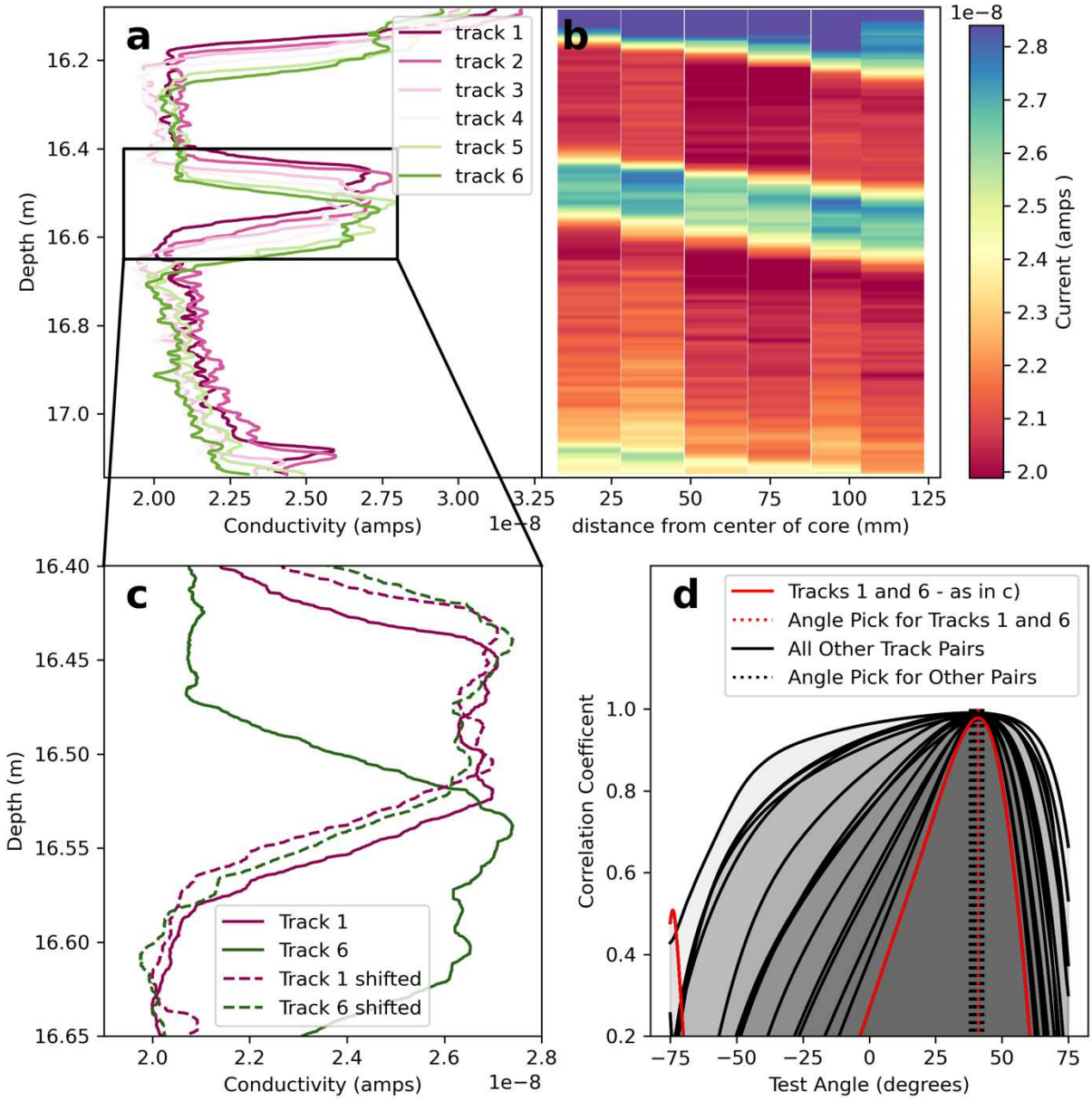

Figure 4. (a) ECM data from a 1-meter section of ALHIC2302. Each line represents a single track, with the shading indicating distance across the core. (b) Same data in top-down view, as with Fig. 2, with the color bar indicating the electrical current. (c) Zoom in of the feature highlighted by the box in (a), showing the depth of tracks 1 and 6 before and after shifting to the angle of maximum correlation between the two tracks. (d) Relationship between the correlation coefficients between pairs of tracks and the text angle, with the tracks 1 and 6 correlation coefficient in red.

The method described below assumes that layer orientations are consistent for the full core section (roughly 1 m in length). It does not attempt to resolve cm-scale folding or disturbances to layering, although a visual evaluation of the data indicates these are not present. We calculate the dip and dip direction from 3D ECM data as follows:

1. *Clean data*: First, we manually process the 3D ECM data, removing sections flagged for poor ice quality or surface defects. We ignore the upper and lower 10 mm of each track as the core ends introduce noise. We also apply a running 10 mm median smoothing.
2. *Compute apparent dip on a single face (δ_1):* We calculate an apparent dip for every pair of tracks on a given face by adjusting the depth of a pair of tracks until the correlation between them is maximized. This depth adjustment is used to calculate an apparent dip angle given the horizontal spacing of the two tracks. In an ideal case, with six tracks per face, there are a total of 15 pairs to test. Notably, cut geometry does limit this to as little as three tracks per face on some sections of ALHIC2201. Electrode contact issues also mean the data from some tracks is unusable.

   For each pair of tracks, we identify the longest section of overlap between tracks maintained across the full range of dip angles to be considered (-75° to 75°). Any length of surface defects on the core noted during data collection is also excluded from the overlap. We do not compute a dip angle for any pair of tracks where this overlap is shorter than 20 cm.

   At each angle from -75° to 75°, at 0.1° increments, we shift the depth record for each track by the track's distance from the center of the core multiplied by the tangent of the angle. Two tracks, before and after this depth shift, can be seen in Fig. 4c. Each track is then interpolated onto a common 1 mm depth vector, and a Pearson correlation coefficient for the pair of tracks is calculated. The results of this calculation for one core section are shown in Fig. 4d. The angle with the largest correlation coefficient is then taken as δ_1, the apparent dip for this pair of tracks. The angle δ_1, the length of the overlap, and the associated correlation coefficient are recorded.
3. *Compute apparent dip on the perpendicular face (δ_2):* We repeat the same process as above on the perpendicular face from the same core section to find δ_2, the second apparent dip.
4. *Compute dip direction (α):* With two sets of apparent dip angles (δ_1 and δ_2) on perpendicular faces, we can determine the 3D orientation of the layering. This is performed for every combination of angle picks from the two faces, which with 15 picks on each face results in 15^2=225 total dip angles (for ideal core sections). If there are less than 3 apparent dip estimates on a given face due to cut geometry or electrode contact issues, we do not proceed with computing a dip direction or dip on this core section. The geometry of dip direction is shown in Fig. 5. Notably, dip direction is positive in the counterclockwise direction, and so describes the angle W of the orientation line.

   We calculate the dip direction as in Equation 1.

$$\alpha = \tan^{-1}\left(\frac{\tan(\delta_2)}{\tan(\delta_1)}\right) \quad (1)$$

5. *Compute dip (δ):* Next we calculate the dip from the horizontal plane as in Equation 2.

$$\delta = tan^{-1}\left(\frac{\tan(\delta_1)}{\cos(\alpha)}\right) \quad 2$$

As with dip direction, there is a total of 225 dip estimates for an ideal core section.

6. *Assign confidence to dip and dip direction estimates:* The length of the two tracks used to calculate each apparent dip estimate and the maximum Pearson correlation coefficient achieved are recorded. For each estimate of dip and dip direction, we compute a confidence score, which is the product of the length and the correlation coefficient of each pair of tracks. This approach ensures that longer sections of overlap (i.e., longer core sections and adjacent tracks that don't require as much shifting to align) are more heavily weighted. Likewise, pairs of tracks which align well, as indicated by a larger correlation coefficient, are more strongly weighted.
7. *Compute weighted-median dip and weighted-mean dip direction:* With the confidence score used as weighting, we calculate the weighted median and interquartile range (IQR for the dip on each section of core. Because dip direction can vary between 0° and 360°, we calculate a weighted circular mean for dip direction, where the weighted mean of the x and y components of the angle is computed, and then combined for an estimate of the dip direction.

We exclude results where the weighted interquartile range on dip is >20°, as visualized in Fig 7.

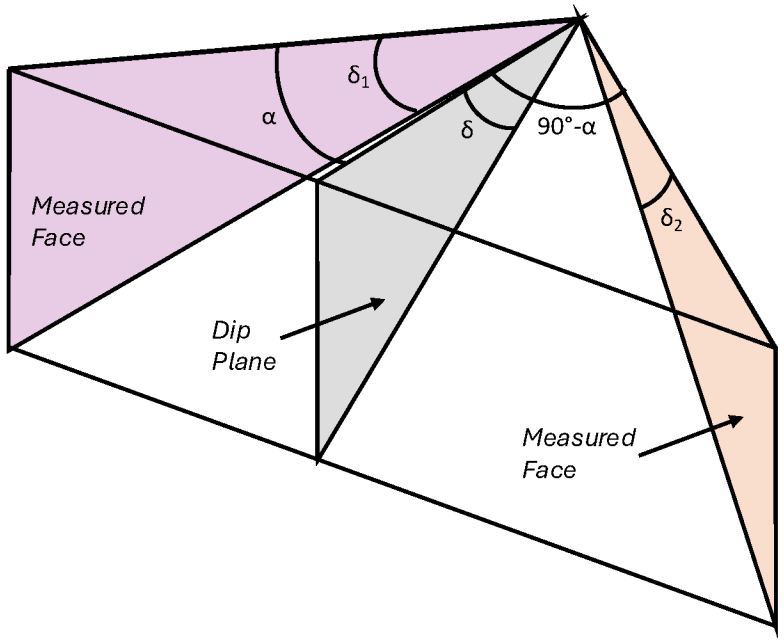

Figure 5. Diagram demonstrates the principal behind the calculation of the three-dimensional layer orientation. Here δ_1 and δ_2 represent the apparent dip in two perpendicular planes, and δ

represents the dip. α represents the angle between the vertical plane aligned with the core's orientation line and the plane of dip. Given that δ_1 and δ_2 are in perpendicular planes, α and δ can both be calculated as a function of δ_1 and δ_2.

3. RESULTS

Both ALHIC2201 and ALHIC2302 show clear layering in both AC and DC measurements. The magnitude of variation in conductance and the thickness of the layers varies among sections. Most layering is not observable with visual inspection, although a visible layer of particles in ALHIC2201 results in a clear low in DC conductivity and a clear peak in AC conductivity (Fig. 6), consistent with neutralized acidity and elevated ion content from a tephra layer.

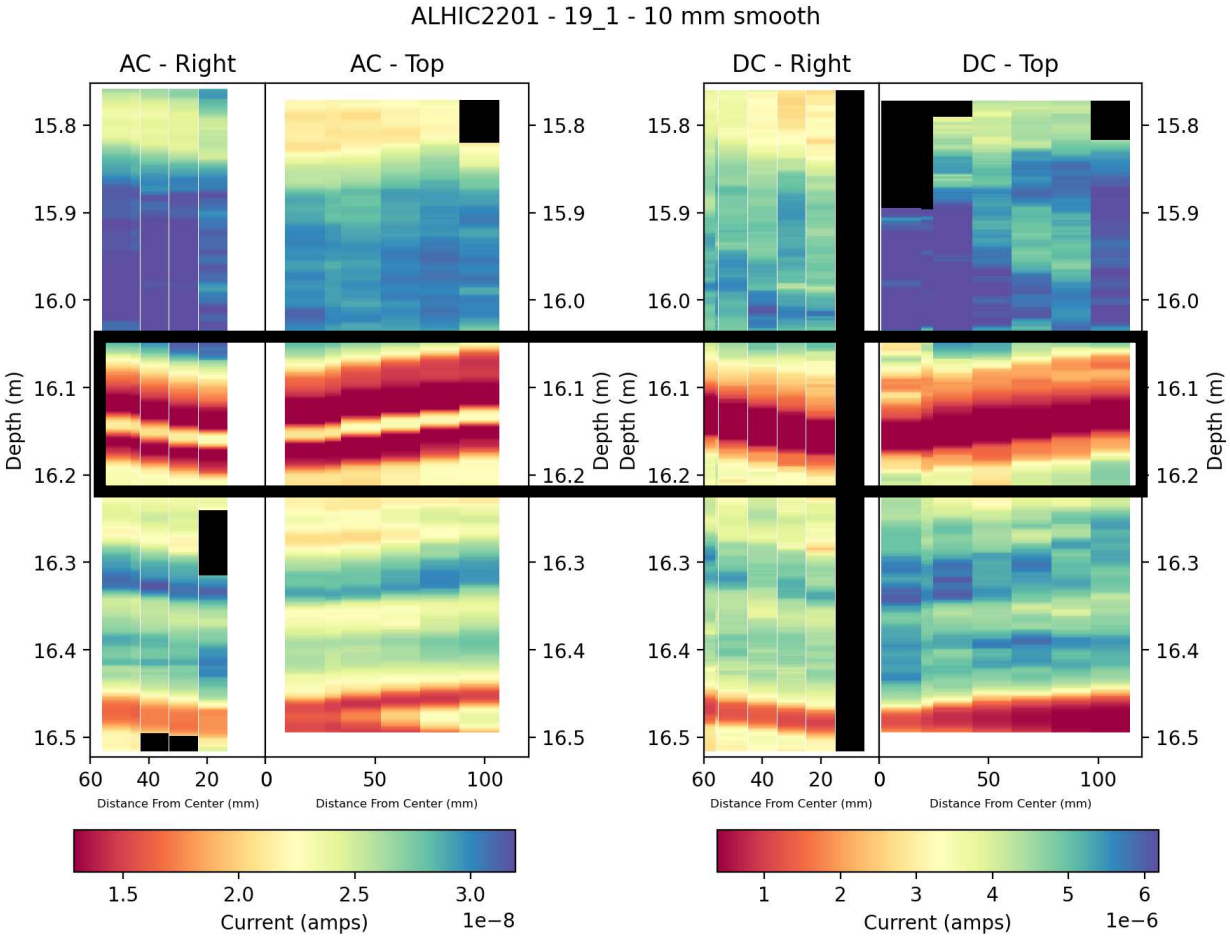

Figure 6. AC and DC ECM data from ALHIC2201 section 19_1. Plots show depth increasing down the y-axis. The x-axis represents distance from center of core, measured from the corner where the two perpendicular faces ("right" and "top") meet. The color bar for AC and DC shown at the bottom of the figure is held consistent on both faces. The outermost tracks (which often have offset magnitudes) are normalized to match the average value of other tracks. The strong layering at 16.15 (highlighted by the black box) is coincident with a faint band of dark particles, but this was only noticed after the reduced DC conductivity and elevated AC conductivity was

noted. This layer, and others in the section, are visibly dipping in both planes. Sections with poor electrode contact are marked in black.

Confident dip estimates which meet the 20° IQR threshold are achieved on 79% of measured core sections. On 14% of measured core sections, there are not 3 or more pairs of tracks with >20 cm of overlapping ECM. This was largely caused by either small cracks impacting electrode contact in shallow ice, or constrained cut geometry limiting the number of tracks in ALHIC2201 due to the prior sampling on this core. The remaining 6% of measured core sections had an IQR spread greater than 20° (and in most cases, much greater). These sections are more homogenous to AC ECM, and so were the most impacted by noise. We observe a bimodal distribution in some sections of ALHIC2302, as seen in Fig. 7, with estimates clustered around both positive and negative steep angles. The reason for this is unclear but may relate to the periodicity of layering being such that a layer can align with the one above/below at the extreme opposite end of the tested range. A similar effect can be seen in Fig. 4d, where there is a secondary peak in correlation strength at strongly negatively dipping values, while the consensus dip angle is strongly positive.

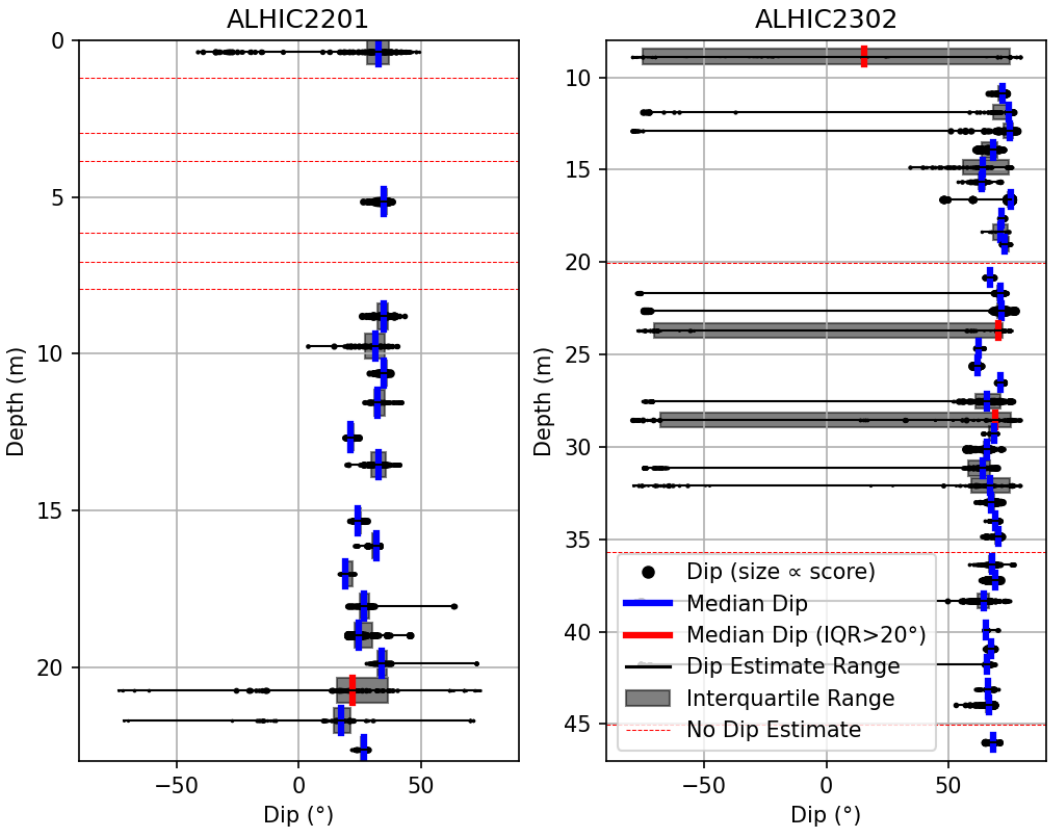

Figure 7. Section dips from ALHIC2201 (left) and ALHIC2302 (right). Individual dip estimates are denoted by dots, where the size is proportional to the confidence score. Depth is shown on the y-axis in meters, and the dip is shown from -90° to 90° on the x-axis. All sections are normalized such that the weighted median is positive. Sections where the interquartile range (IQR, shown

in grey) is <20° are included in further analysis, and marked by a blue line for the weighted median, while the excluded dip calculations are marked by red lines. Sections where no dip estimate was achieved are shown with red dashed lines.

The average dip calculated for ALHIC2201 is 28° with a standard deviation of 6.0°. ALHIC2302 has steeper dips, with an average of 68° and a standard deviation of 3.4°. A t-test indicates statistically significant trends ($p<=0.05$) for both datasets, with the dip decreasing over depth. In Fig. 8, we fit a linear trendline to the median dips and find slopes of -0.56° per m in ALHIC2201 and -0.15° per m in ALHIC2302. This analysis excludes dip estimates where the interquartile range exceeds the 20° threshold.

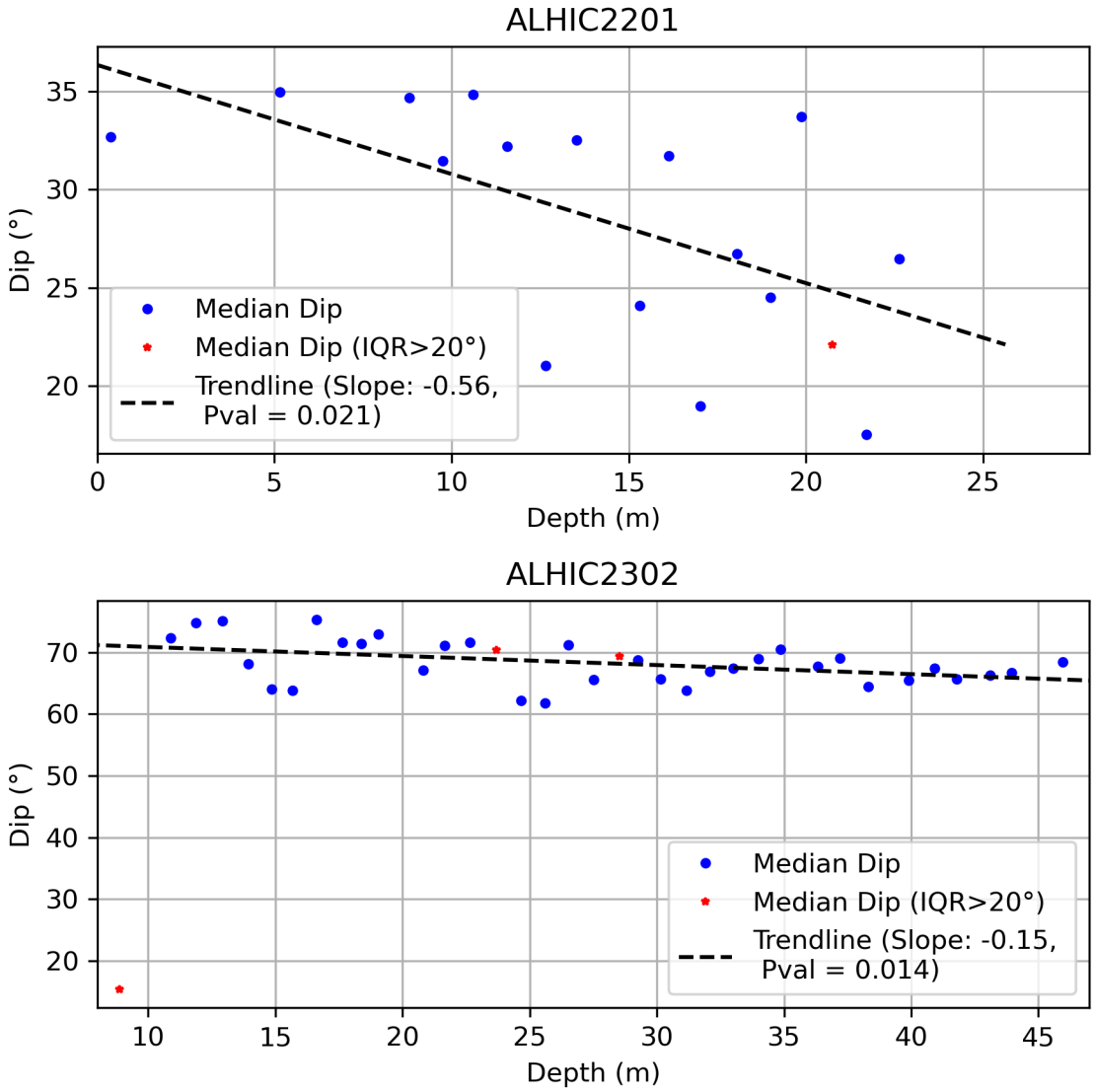

Figure 8. Fitting a trendline to the median dips shows moderate but statistically significant trends with dip. The dip changes by -0.61 and -0.14 ° per m on ALHIC2201 (top) and ALHIC2302 (bottom) respectively. Excluded dip values (where interquartile spread is >20°) are shown with red stars and are not used in the slope calculation.

The dip can be ~10° offset from an adjacent core section, as seen with variations in the dip shown in Fig. 7 (i.e. near 25 m depth in ALHIC2302). These variations exceed the interquartile range of some pairs of adjacent core sections. This may indicate actual changes in layer orientation at these fine scales, but it may also indicate sources of measurement error not captured in the uncertainty presented in the layer dip estimate. The orientation of the core tray and non-perpendicular face cuts both may be responsible for some degree of error but are unlikely to explain the full spread in the data.

We also present the weighted circular mean for dip direction estimates, as shown in Fig. 9, where the weighted mean of the x and y components of the circular data are individually computed and combined into a final angular average. We do not present percentile results, as we do for dip, due to the ambiguity in presenting percentile/median results on circular datasets. For both cores, the orientation of layering is generally consistent (within ~25°) between depths where the core logs note orientation was lost. We suspect the exceptions to this (17-20 m vs. 21-23 m in ALHIC2201, the spread from 10-20m in ALHIC2302) may be driven by errors with transferring the orientation line. The significant changes to dip direction where the orientation was lost is expected, as the position of the orientation line relative to the ice stratigraphy may have changed.

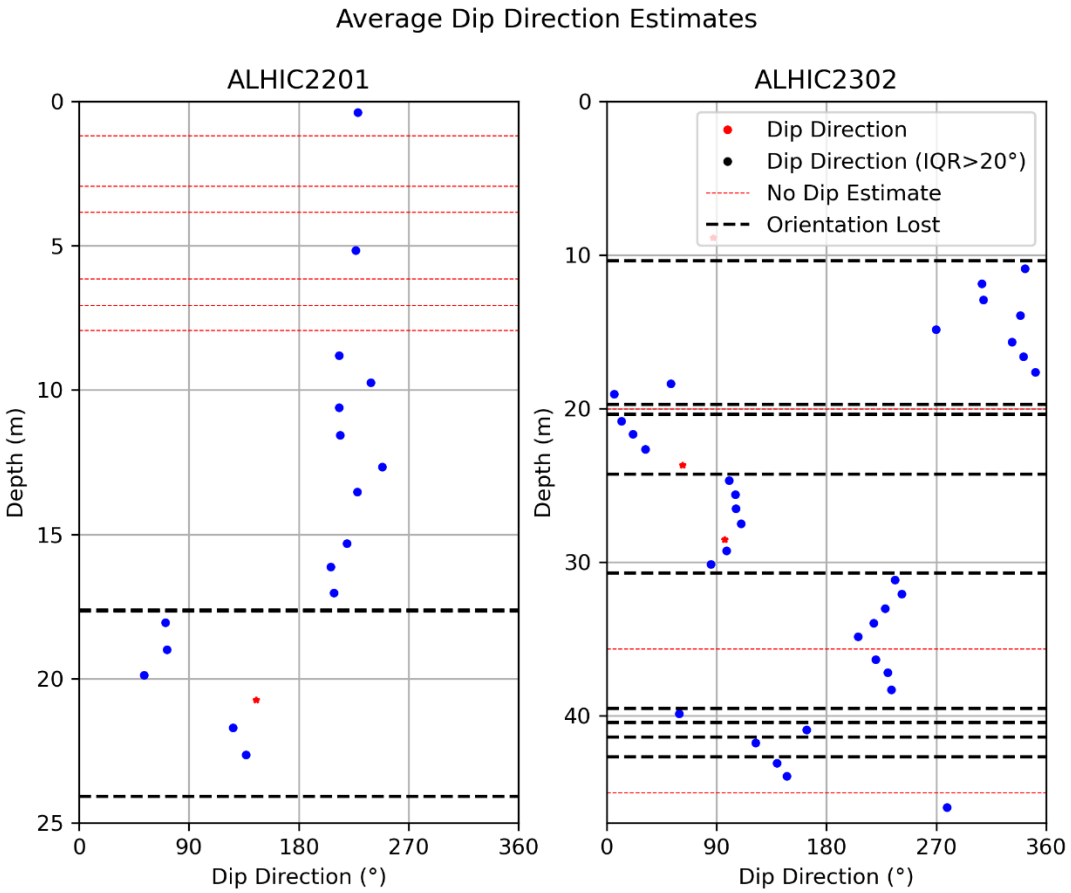

Figure 9. The weighted circular average dip direction is plotted against depth for each section in ALHIC2201 (left) and ALHIC2302 (right). Note that the average dip direction estimate is generally

consistent where drill logs indicate continuous core orientation (core breaks are indicated by the horizontal black dashed lines). Sections where dip cannot be calculated are shown with a red dashed line, and red stars indicate dip direction where the interquartile spread is greater than 20°. Here the calculated dip direction has been rotated by 180° for sections where the median dip is negative.

The azimuth of the orientation line was consistent for the upper 17 m of ALHIC2201. Therefore, dip direction estimates from the uppermost sections of this core can be added to the azimuth of the orientation line to determine the dip azimuth. The dip direction of the upper 17 m of ALHIC2201 is on average 222° W of the orientation line. This orientation line has a measured azimuth of 56° E of N at the surface. Thus, the dip azimuth of this section of ALHIC2201 is 198° E of N. This measurement has significant uncertainty, including +/- 5° on the orientation line GPS azimuth measurement, and a standard deviation of 13° in the dip direction calculations across this measurement range. Determining dip azimuth is not possible on ALHIC2302, as the azimuth of the orientation line was not measured and, even if the azimuth of the orientation line was known at the surface, the orientation was lost above the first 3D ECM dip calculation.

4. DISCUSSION

4.1 Implications for ice core sampling

The combination of steeply dipping layering and large-diameter cores presents new challenges for ice core analysis. In most ice core analysis campaigns, the depth of each sample is carefully measured, but the location of the sample within the core's cross section is not. This is built on the assumption that the layering is near-horizontal, and so multiple measurements at the same depth all sample the same layers. This is not the case in Allan Hills ice. A dip of 70° will result in a single layer having a >0.6 m offset in depth across the width of a large-diameter core. This uncertainty exceeds the sub-centimeter resolution of many modern ice core analysis techniques and complicates the development of multi-proxy records which are assembled from multiple parallel sets of samples.

The combination of 3D ECM and careful logging of the three-dimensional location of each sample enables parallel sets of measurements to be placed on a common depth scale. We recorded this information for samples from ALHIC2302 in advance of an upcoming multi-institution core sampling campaign. Multiple vertical sticks from different locations within the core will be measured for the same parameters to verify the reproducibility of the measurements. The layering imaged with 3D ECM will allow multi-proxy records from Allan Hills cores to have cm-accurate depth alignment similar to conventional ice cores. Unfortunately sampling on ALHIC2201 was completed before 3D ECM measurements were made and accurate depth alignment of samples will not be possible in this core.

4.2 Interpretation of layer orientation

In both ALHIC2201 and ALHIC2302, the layering is coherent with large dips. Both cores show a small but statistically significant trend towards shallower dip with depth. This characterization of dip with depth provides insight into the larger scale stratigraphy at the core sites. While 3D ECM allows the orientation of the sections to be aligned relative to one another, the lack of azimuth

information prevents aligning the sections with other spatial observations without additional constraints. Two conceptual scenarios consistent with the change in dip are illustrated in Fig. 10. Fig. 10a shows larger dips near the surface driven by the bed slope and surface ablation rates; in this scenario the layers become shallower along the ice flow direction. Fig. 10b shows the remaining portion of a fold after the upper part has been removed by ablation; in this scenario, the layers get deeper in the ice flow direction. Both scenarios are consistent with the 3D ECM results and differentiating between them requires additional information.

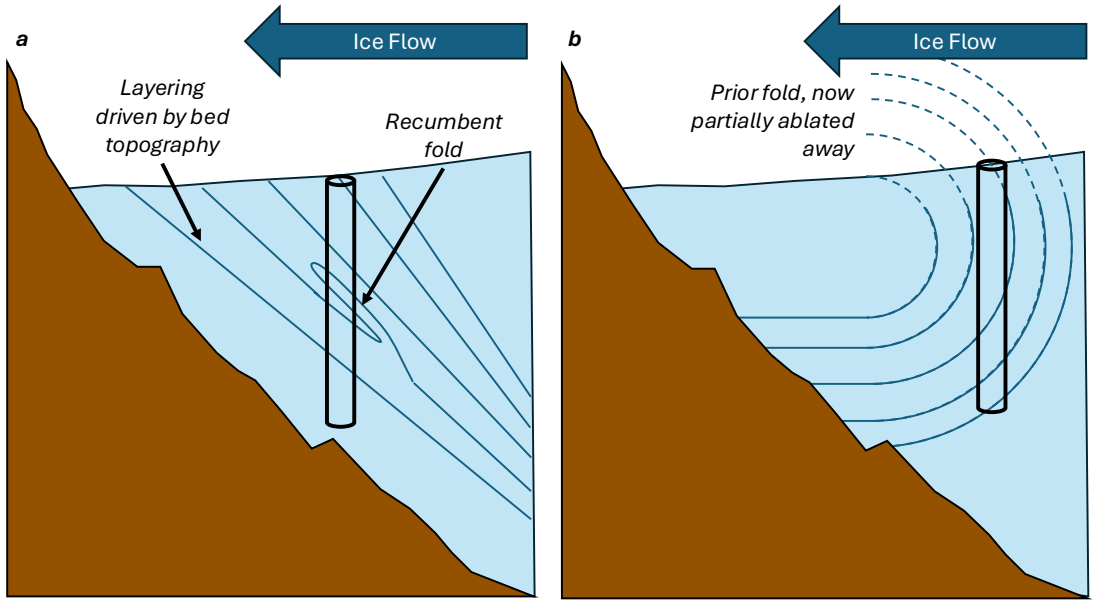

Figure 10. A conceptual sketch depicts two cores in an Allan Hills setting which might produce 3D ECM results consistent with decreasing dips with depth. In the left scenario, layering is largely driven by bed topography. A recumbent fold is included to demonstrate how consistent layer orientation does not guarantee stratigraphic order. In this scenario, layering dips more steeply near the surface, potentially driven by surface ablation. In an alternative scenario on the right, a fold driven by a past flow regime is partially ablated away, resulting in steeply dipping layering. 3D ECM alone cannot conclusively differentiate between these two scenarios.

Ice-penetrating radar data collected in 2019 (Nesbitt and Brook, 2023) provides additional context for these results. While the mismatch between core depths and the radar identification of the bedrock visualized in Fig. 11 indicate some off-axis reflectors may be introducing error into bedrock depth estimates, the radar data provide useful constraints on the bedrock geometry and englacial layering. A radar track (Track 2) perpendicular to the nearby nunatak, which passes the ALHIC2201 drill site, shows englacial layering in the upper 70 m roughly parallel to the bed topography along this track. The apparent dip of the bedrock below the ice core site in this track (28°) is also similar to the average 3D ECM layer dip in ALHIC2201 (29°).

Notably, the azimuth of dip direction for the upper 17m of ALHIC2201 is roughly 45° off this radar track, in the direction of the local bedrock dip as interpolated from the radar data (Fig

11c. This implies the actual bedrock dip may be steeper than dips observed in Track 2 and the 3D ECM data. However, as demonstrated by multiple ice cores exceeding the bed depth estimate (Fig. 11a and 11b), there is significant uncertainty in bed geometry. The combination of englacial layering and bedrock geometry observed in radar data as well the 3D ECM dip and dip azimuth all suggest the englacial stratigraphy in this core is driven by bedrock geometry. Thus, the scenario in Fig. 10a, where layering is parallel with the bed, is well supported for ALHIC2201.

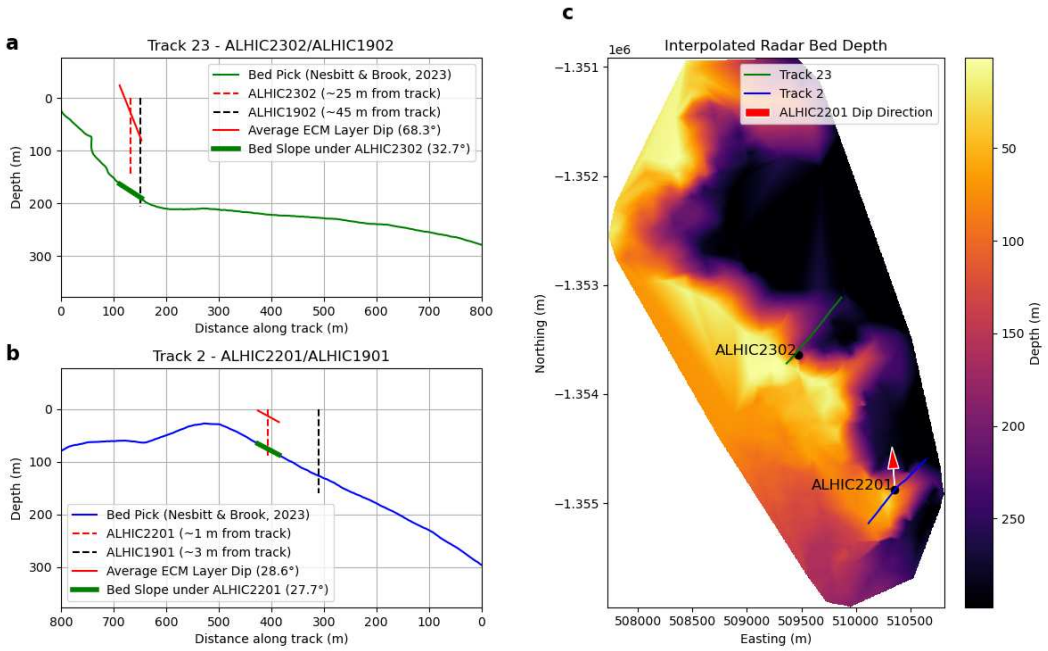

Figure 11. (a) and (b) Bed picks from radar tracks roughly perpendicular to the outcrop at the ALHIC2302 and ALHIC2201 sites. A representation of the two cores drilled close to each site is included, showing their total depth and noting their distance from the radar track. The average ECM layer orientations from this study are shown in red (assuming they dip with the bedrock slope), and the 40-meter average bed slope for each core is shown in green. (c) Interpolated radar bed depths (Nesbitt and Brook, 2023), with the locations of the ALHIC2201 and ALHIC2302 core sites noted (ALHIC1901 and ALHIC2902, respectively, are located so close to the other cores that we omit them for visual clarity). The dip direction azimuth for the upper section of ALHIC2201 is shown with the red arrow. While not parallel to the radar line, it does dip with the local bed topography. As with Fig 1, this plot is oriented with grid north up.

The interpretation of 3D ECM data for ALHIC2302 is less constrained. A radar track roughly perpendicular to the nunatak passes nearby the ALHIC2302 core site, as shown in Fig 11a. This radar track shows bed slopes at 33° near the core site; steep, but significantly less than the 68° dip observed in ECM data. Here, there are no visible englacial layers in the radar data. Therefore, a range of layer geometries, including both conceptual geometries shown in Fig. 10, are possible.

The 3D ECM results presented here also constrain potential folding of englacial layering in both cores. If there were folds with a radius of 5-20 m, we would expect to see 3D ECM dips

steadily increasing to vertical, and then decreasing within the ECM datasets in this study. Such changes are not observed, as the changes to dip angle with depth are gradual. However, there is the potential for folding to still play a role in the layering. For example, a very large fold (as shown in Fig. 10b, with a radius >>20 m, could be consistent with the gradually changing dips in both cores. A small-diameter fold, with a radius on the order of ~1-5m, might be too small for enough 3D ECM measurements to capture the progressive change in dips through the fold. Even smaller radius folds (<1 m radius) would present as curving layering within a single section of 3D ECM data although we do not observe layer curvature or cm-scale folding in the 3D ECM data.

It is also possible for there to be disruptions to the original layering, even if folding is not resolved in the 3D ECM data. Waddington and others (2001) demonstrate the potential for the formation of recumbent folds to form as a result of "wrinkles" in stratigraphy and simple sheer. The authors note these recumbent folds (as portrayed in Fig. 10a might not result in clear disruptions to stratigraphy, even as they represent significant reversals to ice core chronologies. Indeed, in 3D ECM data a recumbent fold would not be distinguishable from other layering. Identification of these features would require additional ice core sampling and dating methods.

4.3 Potential for azimuthal orientation

Determining the azimuth of ice cores has been a long pursued and elusive goal in ice core science. Microstructure and physical properties studies of ice cores often depend on core azimuth to link ice properties to glacier flow, and visa-versa (i.e. Weikusat and others, 2017). Given the significant interest in the glaciological conditions and ice flow necessary for preservation of old ice at the Allan Hills, measurements of ice fabric may provide insight into the current and past ice flow. The fabric information will be more valuable if it can be oriented in space.

The current method for determining ice core azimuth includes aligning the breaks between adjacent core sections to extrapolate a known azimuth down through the core. This method is currently used at the Allan Hills, but core quality limits its utility to the upper meters of the core. Direct azimuth logging during drilling on each core section is difficult to achieve accurately even with modern ice core drilling technology (Fitzpatrick and others, 2014), and is not currently attempted on the large-diameter drill used the Allan Hills. Recent work by Westhoff and others (2021) presents a novel approach combining borehole inclination and azimuth logging with visual line scanning but requires the assumption of flat layering and that the apparent dips are due to the borehole being not perfectly vertical. Allan Hill ice cores have particularly complex layer geometries and challenging core quality such that previous techniques are not applicable.

3D ECM presents a new pathway towards determining ice core azimuth in blue ice regions with complex stratigraphy. With 3D ECM, the dip direction can be determined relative to the core but is not referenced to azimuth. Ground-penetrating radar data can provide the additional information needed to determine ice core azimuth by matching the dip direction from ECM with the dip direction calculated from radar surveys. Because radar data is GPS-referenced, this would enable the determination of the azimuth of the dip direction in Allan Hills cores, and so the orientation of the cores themselves.

This effort will require a dedicated radar campaign, employing a high frequency radar system (~200 MHz) to clearly image layering in the upper 70 meters. Current Allan Hills radar

data, collected with 100 MHz antennas, does resolve some layering dipping roughly in line with the bed above ALHIC2201 (Nesbitt and Brook, 2023). However, this data is not sufficient to clearly resolve layer dip angles. Avoiding spatial aliasing, and so enabling accurate migration after data collection, will require sub-meter posting intervals and so very slow collection speeds (Holschuh and others, 2014). A radar campaign designed to provide perpendicular scans of englacial stratigraphy across the depth range where 3D ECM measurements have been obtained is possible as part of future field work in the Allan Hills.

CONCLUSION

Here we present a novel 3D ECM method for imaging layering in ice cores. We compute the apparent dip on two perpendicular faces of an ice core by finding the depth offset between parallel ECM tracks. Combining the apparent dip on both perpendicular faces enables the computation of both dip and dip direction, uniquely defining layer orientations. We use the spread of estimates from each pair of tracks on both faces to constrain the uncertainty.

3D ECM measurements on ALHIC2201 and ALHIC2302 identify consistent and sloping layering in both cores. Radar data supports the interpretation that the layers in ALHIC2201, with a dip of 27°, are likely parallel to local bed geometry. The steeper layering in ALHIC2302 might be driven by the steeper bed topography at this site, although a lack of constraints on englacial layering from radar data means more complex layer orientations cannot be ruled out. Both cores show a gradual trend towards less steeply dipping layering with depth.

3D ECM promises to be useful to a range of future ice core interpretation efforts. Combined with dedicated radar surveys, 3D ECM might enable the determination of the azimuth of each core section, useful in physical properties studies. 3D ECM also will enable depth alignment of multiple sets of parallel sampling, where the layer dip would otherwise introduce significant uncertainty of relative depth scales.

DATA AVALIBILITY

The 3D ECM data for this project, along with plots of all core sections and the code used in this analysis, will be made available at USAP.gov. Currently, code and data can be accessed on GitHub at https://github.com/liamkirkpatrick/3d_ecm.

AUTHOR CONTRIBUTION STATEMENT

LK collected all 3D-ECM data, led the analysis, and wrote most of the paper. TF assisted in the experiment design, analysis, and paper writing. SS, JMP, and AC logged cores in the field and provided notes on the orientation line. All authors contributed to core processing at the National Science Foundation (NSF) Ice Core Facility.

AKNOWLEDGEMENTS

This work was supported by the U.S. National Science Foundation (NSF) Center for Oldest Ice Exploration (NSF COLDEX), an NSF Science and Technology Center (NSF 2019719), and by NSF grant 2149518. We thank the NSF Office of Polar Programs, the NSF Office of Integrative Activities, and Oregon State University for financial and infrastructure support, and the NSF Antarctic Infrastructure and Logistics Program, the NSF Ice Drilling Program, the NSF Ice Core

Facility, and the Antarctic Support Contractor for logistical support. We thank the NSF Ice Drilling Program for support activities through NSF Cooperative Agreement 1836328.

In addition to the named authors, we appreciate the contributions of additional members of the 2022-2023 Allan Hills field team (Science Team: Jacob Morgan, Peter Neff, Yuzhen Yan. Drillers: Elizabeth Morton, Michael Jayred. Support Staff: Johnathan Hayden.) and the 2023-2024 Allan Hills field team (Science Team: Abigail Hudak, Asmita Banerjee, Edward Brook, John Higgins, John-Morgan Manos. Drillers: Elizabeth Morton, Michael Jayred. Support Staff: Ashley Goverman, Emalia Mayo.). We also thank NSF COLDEX project members who contributed the 2023 and 2024 COLDEX Core Processing Lines and Jacob Chalif for editing assistance.

COMPETING INTERESTS

The authors declare none.

REFERENCES

Alley RB, Gow AJ, Meese DA, Fitzpatrick JJ, Waddington ED and Bolzan JF (1997) Grain-scale processes, folding, and stratigraphic disturbance in the GISP2 ice core. *Journal of Geophysical Research: Oceans* **102**(C12), 26819–26830. doi:10.1029/96JC03836.

Bender ML, Barnett B, Dreyfus G, Jouzel J and Porcelli D (2008) The contemporary degassing rate of 40Ar from the solid Earth. *Proceedings of the National Academy of Sciences* **105**(24), 8232–8237. doi:10.1073/pnas.0711679105.

Bindschadler R and others (2008) The Landsat Image Mosaic of Antarctica. *Remote Sensing of Environment* **112**(12), 4214–4226. doi:10.1016/j.rse.2008.07.006.

Faria SH, Freitag J and Kipfstuhl S (2010) Polar ice structure and the integrity of ice-core paleoclimate records. *Quaternary Science Reviews* **29**(1), 338–351. doi:10.1016/j.quascirev.2009.10.016.

Fischer H and others (2013) Where to find 1.5 million yr old ice for the IPICS 'Oldest-Ice' ice core. *Climate of the Past* **9**(6), 2489–2505. doi:10.5194/cp-9-2489-2013.

Fitzpatrick JJ and others (2014) Physical properties of the WAIS Divide ice core. *Journal of Glaciology* **60**(224), 1181–1198. doi:10.3189/2014JoG14J100.

Fudge TJ, Taylor KC, Waddington ED, Fitzpatrick JJ and Conway H (2016) Electrical stratigraphy of the WAIS Divide ice core: Identification of centimeter-scale irregular layering. *Journal of Geophysical Research: Earth Surface* **121**(7), 1218–1229. doi:10.1002/2016JF003845.

Fudge TJ and others (2013) Onset of deglacial warming in West Antarctica driven by local orbital forcing. *Nature* **500**(7463), 440–444. doi:10.1038/nature12376.

Hammer CU (1980) Acidity of Polar Ice Cores in Relation to Absolute Dating, Past Volcanism, and Radio–Echoes. *Journal of Glaciology* **25**(93), 359–372. doi:10.3189/S0022143000015227.

Higgins JA and others (2015) Atmospheric composition 1 million years ago from blue ice in the Allan Hills, Antarctica. *Proceedings of the National Academy of Sciences* **112**(22), 6887–6891. doi:10.1073/pnas.1420232112.

Holschuh N, Christianson K and Anandakrishnan S (2014) Power loss in dipping internal reflectors, imaged using ice-penetrating radar. *Annals of Glaciology* **55**(67), 49–56. doi:10.3189/2014AoG67A005.

Jansen D and others (2016) Small-scale disturbances in the stratigraphy of the NEEM ice core: observations and numerical model simulations. *The Cryosphere* **10**(1), 359–370. doi:10.5194/tc-10-359-2016.

Karlsson NB and others (2018) Glaciological characteristics in the Dome Fuji region and new assessment for "Oldest Ice". *The Cryosphere* **12**(7), 2413–2424. doi:10.5194/tc-12-2413-2018.

Kuhl TW, Johnson JA, Shturmakov AJ, Goetz JJ, Gibson CJ and Lebar DA (2014) A new large-diameter ice-core drill: the Blue Ice Drill. *Annals of Glaciology* **55**(68), 1–6. doi:10.3189/2014AoG68A009.

Meese DA and others (1997) The Greenland Ice Sheet Project 2 depth-age scale: Methods and results. *Journal of Geophysical Research: Oceans* **102**(C12), 26411–26423. doi:10.1029/97JC00269.

Mojtabavi S and others (2020) A first chronology for the East Greenland Ice-core Project (EGRIP) over the Holocene and last glacial termination. *Climate of the Past* **16**(6), 2359–2380. doi:10.5194/cp-16-2359-2020.

Nesbitt I and Brook E (2023) I-165-M GPR Field Report 2019-2020. doi:10.15784/601669.

Rasmussen SO and others (2013) A first chronology for the North Greenland Eemian Ice Drilling (NEEM) ice core. *Climate of the Past* **9**(6), 2713–2730. doi:10.5194/cp-9-2713-2013.

Rasmussen SO and others (2006) A new Greenland ice core chronology for the last glacial termination. *Journal of Geophysical Research: Atmospheres* **111**(D6). doi:10.1029/2005JD006079.

Severi M, Udisti R, Becagli S, Stenni B and Traversi R (2012) Volcanic synchronisation of the EPICA-DC and TALDICE ice cores for the last 42 kyr BP. *Climate of the Past* **8**(2), 509–517. doi:10.5194/cp-8-509-2012.

Spaulding NE and others (2013) Climate archives from 90 to 250 ka in horizontal and vertical ice cores from the Allan Hills Blue Ice Area, Antarctica. *Quaternary Research* **80**(3), 562–574. doi:10.1016/j.yqres.2013.07.004.

Sugiyama K and others (2000) Measurement of electrical conductance in ice cores by AC-ECM method. *Physics of Ice Core Records*, 173–184.

Svensson A and others (2005) Visual stratigraphy of the North Greenland Ice Core Project (NorthGRIP) ice core during the last glacial period. *Journal of Geophysical Research: Atmospheres* **110**(D2). doi:10.1029/2004JD005134.

Takata M, Iizuka Y, Hondoh T, Fujita S, Fujii Y and Shoji H (2004) Stratigraphic analysis of Dome Fuji Antarctic ice core using an optical scanner. *Annals of Glaciology* **39**, 467–472. doi:10.3189/172756404781813899.

Taylor KC and others (2004) Dating the Siple Dome (Antarctica) ice core by manual and computer interpretation of annual layering. *Journal of Glaciology* **50**(170), 453–461. doi:10.3189/172756504781829864.

Taylor KC, Alley RB, Lamorey GW and Mayewski P (1997) Electrical measurements on the Greenland Ice Sheet Project 2 Core. *Journal of Geophysical Research: Oceans* **102**(C12), 26511–26517. doi:10.1029/96JC02500.

Taylor KC and others (1993) Electrical conductivity measurements from the GISP2 and GRIP Greenland ice cores. *Nature* **366**(6455), 549–552. doi:10.1038/366549a0.

Taylor KC and Alley RB (2004) Two-dimensional electrical stratigraphy of the Siple Dome (Antarctica) ice core. *Journal of Glaciology* **50**(169), 231–235. doi:10.3189/172756504781830033.

Waddington ED, Bolzan JF and Alley RB (2001) Potential for stratigraphic folding near ice-sheet centers. *Journal of Glaciology* **47**(159), 639–648. doi:10.3189/172756501781831756.

Weikusat I and others (2017) Physical analysis of an Antarctic ice core—towards an integration of micro- and macrodynamics of polar ice*. *Philosophical Transactions of the Royal Society A: Mathematical, Physical and Engineering Sciences* **375**(2086), 20150347. doi:10.1098/rsta.2015.0347.

Westhoff J and others (2021) A stratigraphy-based method for reconstructing ice core orientation. *Annals of Glaciology* **62**(85–86), 191–202. doi:10.1017/aog.2020.76.

Wilhelms F (2005) Explaining the dielectric properties of firn as a density-and-conductivity mixed permittivity (DECOMP). *Geophysical Research Letters* **32**(16). doi:10.1029/2005GL022808.

Wilhelms F, Kipfstuhl J, Miller H, Heinloth K and Firestone J (1998) Precise dielectric profiling of ice cores: a new device with improved guarding and its theory. *Journal of Glaciology* **44**(146), 171–174. doi:10.3189/S002214300000246X.

Wolff E, Brook E, Dahl-Jensen D, Fujii Y, Lipenkov VY and Severinghaus J (2006) White paper: The oldest ice core: A 1.5 million year record of climate and greenhouse gases from Antarctica. https://icedrill.org/library/white-paper-oldest-ice-core-15-million-year-record-climate-and-greenhouse-gases-antarctica.

Wolff E (2000) Electrical stratigraphy of polar ice cores : principles, methods, and findings. *Physics of Ice Core Records*. Hokkaido University Press, Hokkaido, Japan, 155–171. http://hdl.handle.net/2115/32467.

Wolff E, Basile I, Petit J-R and Schwander J (1999) Comparison of Holocene electrical records from Dome C and Vostok, Antarctica. *Annals of Glaciology* **29**, 89–93. doi:10.3189/172756499781820888.

Yan Y and others (2019) Two-million-year-old snapshots of atmospheric gases from Antarctic ice. *Nature* **574**(7780), 663–666. doi:10.1038/s41586-019-1692-3.